How to cite: *Angew. Chem. Int. Ed.* **2023,** *62,* e202300413
International Edition: doi.org/10.1002/anie.202300413
German Edition: doi.org/10.1002/ange.202300413

VIP **Single-molecule Magnets** **Very Important Paper**

Nanostructuring of Rare-earth-based Single-Molecule Magnets as Long-range Ordered Arrays in the Framework of Organic Metal Halide Perovskites

Congcong Chai, Junyan Zhou, Munan Hao, Qi Li, Jiali Lu, Shifeng Jin, and Xiaolong Chen**

Abstract: The nanostructuring of single-molecule magnets (SMMs) on substrates, in nanotubes and periodic frameworks is highly desired for the future magnetic recording devices. However, the ability to organize SMMs into long-range ordered arrays in these systems is still lacking. Here, we report the incorporation of magnetic $(RECl_2(H_2O)_6)^+$ (RE = rare earths) molecular groups into the framework of an organic metal halide perovskite (OMHP)—$(H_2dabco)CsCl_3$. Intriguingly, we show the incorporated rare-earth groups self-organized into long-range ordered arrays that uniformly and periodically distributed in the A sites of OMHP. The ordered $(RECl_2(H_2O)_6)^+$ groups serve as SMMs in the perovskite frameworks, exhibiting large effective magnetic moment, moderate magnetic anisotropy and two-step relaxation behavior. With the additional merit of great structural flexibility and multifunction of OMHPs, the preparation of the first SMMs@OMHP magnetic materials furthers the development of molecular spintronics.

Single-molecule magnets (SMMs) have been extensively investigated over the past two decades for their potential applications in the field of high-density data storage, molecular spintronics, and quantum calculation.[1] Unlike traditional ferromagnetic materials, the magnetism of SMMs is derived from the magnetic moment of a single molecule,[2] which has little, if any, interaction with their adjacent magnetic moments. Therefore, the advantage of SMMs lies in their ability to possess magnetic bistate at molecular levels, lifting the domain size limit on the memory density in comparison with their inorganic counterparts.[3] Since the discovery of the first SMM Mn12 in the early 1990s,[4] a number of SMMs with high blocking temperature (T_B) have been synthesized by controlling the ligand field around the rare-earth ions.[5] The choose of different organic ligands or substrates also leads to multifunctional SMMs, in which magnetism and other physical properties, such as luminescence, conductance and chirality, are correlated.[6]

From the point of practical application, SMMs need to possess a T_B around room temperature, and be arranged in ordered 2D or 3D nanostructures on a substrate or within a host to allow for read-and-write processes and to avoid environmental damages.[7] Despite the recent impressive breakthroughs in extending the T_B of SMMs beyond liquid-nitrogen temperatures,[8] efforts to direct deposition of SMMs materials on different substrates to fabricate memory devises often leads to sample decomposition, or the uncontrollable order/orientation of SMMs molecules.[9] Subsequently, interests are arising to insert the SMMs into various porous materials with confined chemical environments, most notably mesoporous silicas,[10] and carbon nanotubes.[11] Assembling SMMs into such porous materials can achieve a nanoscale density without destroying the functionality of materials, but the SMMs are only ordered in short ranges.[11] More recently, metal–organic frameworks (MOFs) are proposed as more ideal templates for long-range nanostructuring of Mn-based SMMs.[12] However, while the periodically ordered framework of MOFs is preserved during the absorption, the absorbed SMMs itself is shown to occupy the sites only partially and in a random manner, leading to disordered distribution of the SMMs.[4,9b,11,12] Thus, the controlling of long-range ordering of SMMs on substrates and especially in protective chemical frameworks continues to be a significant challenge in this research field.

[*] C. Chai, Dr. J. Zhou, M. Hao, Q. Li, J. Lu, Prof. Dr. S. Jin, Prof. Dr. X. Chen
Beijing National Laboratory for Condensed Matter Physics, Institute of Physics, Chinese Academy of Sciences
Beijing 100190 (China)
E-mail: shifengjin@iphy.ac.cn
chenx29@iphy.ac.cn

C. Chai, M. Hao, Q. Li, J. Lu
College of Materials Science and Opto-Electronic Technology, University of Chinese Academy of Sciences
Beijing 101408 (China)

Dr. J. Zhou, Prof. Dr. S. Jin, Prof. Dr. X. Chen
School of Physical Sciences, University of Chinese Academy of Sciences
Beijing 101408 (China)

Prof. Dr. X. Chen
Songshan Lake Materials Laboratory
Dongguan 523808 (China)

Organic metal halide perovskite (OMHP) with general chemical formula "ABX_3" is one of the most widely studied framework structures due to its highly tunable crystal structures and excellent electrical, optical, and dielectric properties.[13] This is largely owing to the A site's high tolerance to accommodate a variety of molecular species. OMHPs hence have a great flexibility in terms of device design.[14] The low-temperature solution-processability also makes OMHPs promising materials for low-cost and large-area preparation. Unfortunately, up to now there has been no report of success in incorporating SMMs into perovskite frameworks. Since isolated SMMs can reach tens of angstroms in size,[7,12a] it is extremely difficult to host them in the A sites for most OMHPs. New strategy is still needed to explore the OMHPs-based SMMs.

In this study, we first construct a rare-earth-contained molecular group of proper size and valence to be inserted into the A sites of an OMHP. The rare earths (RE) should be in an asymmetric crystal field so as to increase anisotropic magnetization. $(RECl_2(H_2O)_6)^+$ is a good choice in terms of these requirements. Then we test $(H_2dabco)CsCl_3$ as a potential host OMHP in which $(H_2dabco)^{2+}$ ions are expected to be partially replaced by the rare-earth groups. Here we show that this strategy works and leads us to successfully synthesize a series of perovskites, $(RECl_2(H_2O)_6)_2(H_2dabco)_7\ Cs_9Cl_{25}V_{Cl2}$ (RE (1), RE = rare earths except Sc/Pm/Lu, dabco = 1,4-diazabicyclo [2.2.2] octane, and V_{Cl} = anion vacancy). According to our best knowledge, this is the first report of introducing rare-earth elements into the A sites of OMHPs. Millimeter-sized and air-stable crystals can be grown simply by evaporative crystallization from aqueous solutions at room temperature (inset of Figure S1). Importantly, unlike SMMs that physically absorbed onto MOFs or carbon nanotubes, the incorporated rare-earth groups that ionically bonded to the perovskite frameworks is uniformly nanostructured and with precise long-range order. Results of magnetic and electron density measurements show that the so introduced rare-earth groups are SMMs occupying the A sites of the OMHP orderly. The average size occupied by each rare-earth group is in nanometer level, $\approx 1.37\ nm^3$, and the high density of SMMs in OMHP is also superior to that of mesoporous frameworks.[12a,c]

The structure of the parent compound $(H_2dabco)CsCl_3$ determined by single-crystal X-ray diffraction (SCXRD)[15] is shown in the left diagram of Figure 1 (partial) and Figure S2 (full). The $CsCl_6$ octahedra connect each other via corner linkage, forming a 3-dimensional network with $(H_2dabco)^{2+}$ molecules occupying the interstitial sites. It belongs to the perovskite structure with space group $C2/c$.[15] Upon partial substitution of $(H_2dabco)^{2+}$ by heterovalent $(RECl_2(H_2O)_6)^+$, a series of compounds RE (1) are obtained and their crystal structures are determined using powder X-ray diffraction (PXRD) and SCXRD. The elemental analysis is performed using energy dispersive spectroscopy (EDS) (Figure S3). Since all the RE (1) compounds are isostructural (Figure S4 and Table S1), we here take Dy (1) as a typical example to describe the structures and magnetic properties in details. Dy (1) crystallizes in triclinic $P\bar{1}$ space group at 298 K[16] (Figure S1) and shows a pseudo $R\bar{3}$ symmetry (Figure S5 and S6), see Table S2. The visualization of the crystal structure was performed using Vesta software.[17] The Dy (1) can be best described as a defective organic–inorganic hybrid perovskite structure (Figure 2(a)) with the general formula $A_2A'_7B_9X_{25}V_{Cl2}$ (A is monovalent rare-earth group, A′ divalent organic ammonium, B monovalent alkali metal, X halogen element and V_{Cl} anion vacancy). The results of elemental analysis also confirmed the element ratio Cl:Cs:RE = 29:9:2 (Figure S3). The mismatch in the valence between the rare-earth groups and $(H_2dabco)^{2+}$ leads to the formation of Cl^- vacancies. No obvious structural phase transitions are observed from 5 K to 273 K based on the variable temperature PXRD measurements (Figure S7).

The A sites of this hybrid perovskite compound consist of three different moieties: monovalent rare-earth groups, disordered diprotonated dabco molecules and ordered diprotonated dabco molecules, with molar ratios 2:1:6. The structures of these three moieties are shown in Figure 2(a) and Figure S8. The Dy^{3+} ion is bonded by six O atoms at 2.352–2.437 Å and two Cl^- ions at 2.6858–2.7108 Å. The peak around 3400 cm^{-1} in Raman spectrum suggests the presences of H_2O molecules (Figure S9). Differential charge density analysis clearly shows two H peaks around each O atom (inset of Figure S9), suggesting the $(DyCl_2(H_2O)_6)^+$ groups are highly ordered within the framework. Intriguingly, the refined structure model suggests the substituted Dy groups self-organized into layered honeycomb superlattice within the perovskite framework (Figure 2(b)). As a consequence of $(DyCl_2(H_2O)_6)^+$ substitution, equal number of Cl^- vacancies appeared as defective octahedrons ($CsCl_5V_{Cl}$), and are bonded to Cl^- anions in Dy groups to compensated the charge (Figure 2(c)). The bonding with two ($CsCl_5V_{Cl}$) octahedrons organizes the Dy groups into pairs about 9.27 Å apart (Figure 2(b) and 2(c)). In addition, the sites between the charge compensated octahedrons ($CsCl_5V_{Cl}$) should be occupied by divalent $(H_2dabco)^{2+}$ groups. These structural requirements organized the Dy groups into a honeycomb lattice within the *ab* plane, which is perpendicular to the direction of the pseudo threefold rotation axis *c** (easy magnetization axis, as shown in the following section) (Figure 2(b), Figure S10 and Table S3). Due to the larger volume of RE groups and the presence of Cl vacancies, the $CsCl_6$ octahedrons in the framework of Dy (1) distort significantly. The bond lengths of Cs–Cl cover a notably narrow range from 3.333 to 3.439 Å in the parent

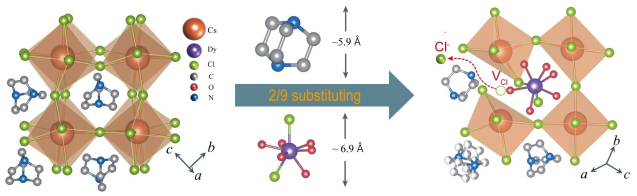

Figure 1. The design scheme for incorporating single-molecule magnets into organic metal halide perovskite frameworks by partially substituting organic molecules in the A sites with rare-earth groups.

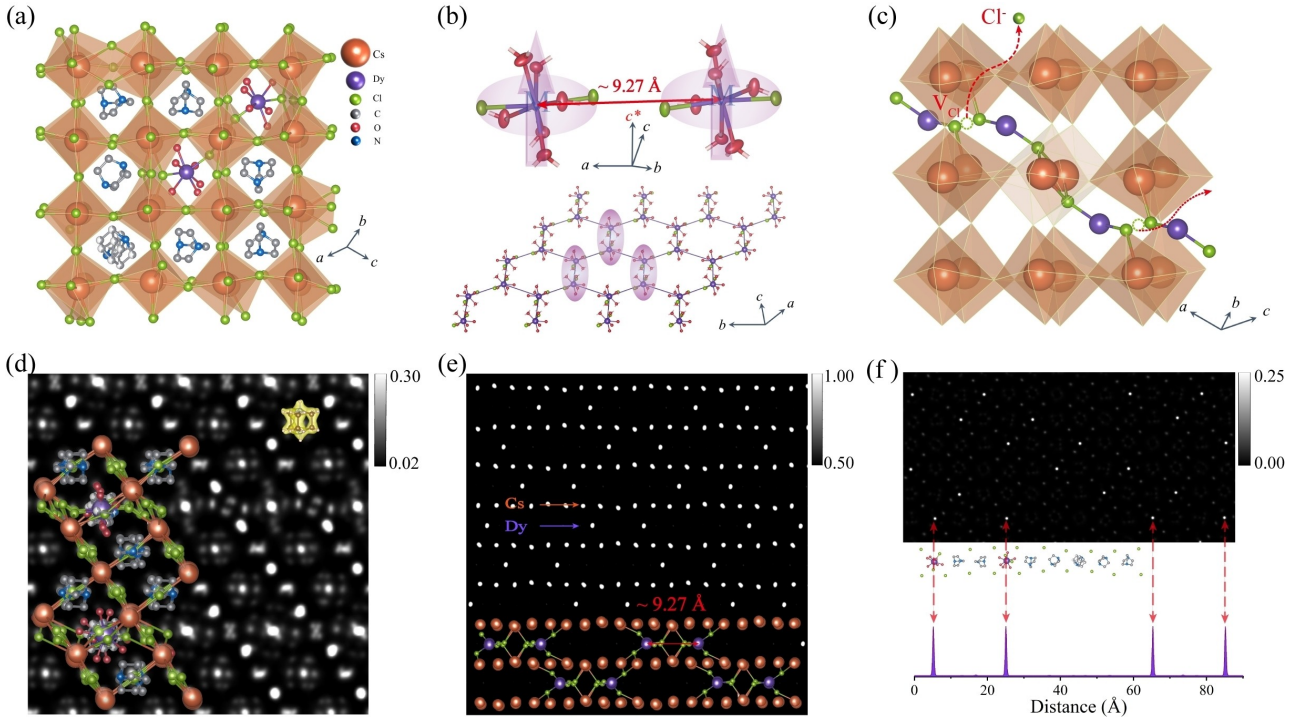

Figure 2. Crystal structures. (a) Crystal structures of Dy (1). (b) Top: orientation of the rare-earth groups and the easy-magnetization direction. *c** is the *c* axis of the pseudo $R\bar{3}$ lattice; Bottom: the hexagonal honeycomb layer structure formed by self-organized Dy pairs. (c) Details of highly distorted $CsCl_6$ octahedra and the resulting Cl^- vacancies. The projection of EDDs along the direction of zone axis (d) [120] and (e) [011]. The superimposed structural model is obtained through single crystal structure determination. (f) The electron density distributions across the A-sites of this perovskite. In the picture above, the brightest spots are ordered Dy ions on A-sites. Below, electron density across an array of A sites, the intensity is found neglectable on sites occupied by organic molecules. The scale labels on the right side of Figure 2(d)–(f) show the normalized EDDs values.

compound, while 3.2940–3.6217 Å in Dy (1) (Table S4), which shows the complexity of coordination of B-site atoms of the latter. Between every two Dy honeycomb layers, the voids of the framework are also complemented by two layers of (H_2dabco) groups (Figure S11). Therefore, the self-organization of charged Dy groups within the defective perovskite framework ensured an ordered nanostructuring of the Dy-contained groups in the framework of OMHPs.

To visualize the Dy guest molecules in porous OMHPs without any assumptions based on models, the electron density distributions (EDDs) of Dy (1) was constructed based on maximum-entropy method (MEM) from SCXRD data with Dysnomia.[18] The determined EDDs have high precision ($wR_F = 0.016$), and the results agree well with the model obtained from structure refinement (Figure 2(d)). Figure 2(e) shows the projection of EDDs along the direction of zone axis [011], in a scale that only the heaviest Cs and Dy atoms are clearly seen. The Dy pairs in a distance of 9.27 Å apart are clearly visible. The EDDs across the A-sites of this perovskite were analyzed separately (Figure 2-(f)). While the EDDs of the RE groups are concentrated on the centered Dy atoms, that of the organic molecules are more diffuse, so that the Dy become the brightest atoms in quasi-square Cl sub-lattices (dimmed spots in Figure 2(f)). Similarly, a significant distortion of the Cl lattices is clearly visible around the Dy pairs. Meanwhile, the EDDs along the direction of Dy arrays are extracted, as given in the bottom of Figure 2(f), and a highly ordered spatial arrangement of Dy atoms is revealed. Through the results of EDDs analysis, we convincingly show the incorporated RE groups self-organized into ordered arrays that uniformly and periodically distributed in the A sites of OMHP.

The DC magnetic susceptibility was measured in temperature range of 2–300 K and with a 5 T field perpendicular to the *ab* plane of the Dy (1) single crystal (Figure 3(a)). The inverse susceptibility χ obeys the Curie–Weiss law $\chi^{-1} = (T-\theta)/C$ above 50 K, and deviates significantly below 50 K. The results of fitting are given in Figure 3(a), with a Curie constant $C = 14.04\ \mathrm{K\,mol^{-1}\,Oe^{-1}}$ and Weiss temperature $\theta = 21.55$ K. The effective magnetic moment is calculated to be $\mu_{\mathrm{eff}} = 10.60\,\mu_B$/Dy, agreeing well with the theoretical value 10.63 μ_B/Dy calculated from the formula $g_J\sqrt{J(J+1)}$. The χT vs. T data firstly rises from 300 K to 20 K, and then drops drastically after reaching its maximum (Figure S12), showing an "up-down" pathway upon cooling. The increase in χT upon cooling suggests the presence of ferromagnetic coupling in Dy (1), which may be caused by short-range super-exchange effect within the paired Dy ions.[6a,19]

When H is perpendicular to the *ab* plane, the magnetization increases drastically in the range of 0–0.5 T at 2 K, and reaches a saturated value of $\approx 10\,\mu_B$/Dy below 1 T

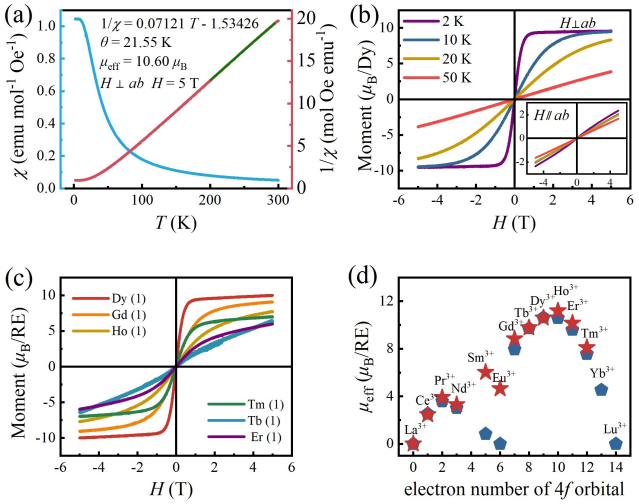

Figure 3. DC magnetic susceptibility. (a) Temperature dependence of magnetization measured at 5 T between 2 and 300 K. The olive line shows the Curie–Weiss fitting between 200–300 K. (b) Isothermal magnetization versus external magnetic field for Dy (1) measured at selected temperatures, magnetic field applied perpendicular to the *ab* plane and along *ab* plane (shown in inset), respectively. (c) Isothermal magnetization versus external magnetic field measured at 2 K for compounds with other rare-earth elements. (d) Comparison of the effective magnetic moments between experiment values in this article (red pentacle) and theoretical predictions based on spin-orbit coupling (blue pentagon).

(Figure 3(b)). A small magnetic hysteresis (≈20 Oe) is observed in the *M-H* loop in the low fields. SMMs with nearly negligible hysteresis like Dy (1) have been reported before.[20] At 50 K, the linear magnetization dependence on field suggest that the paramagnetism dominate. In comparison, when H is parallel to the *ab* plane, the magnetization keeps increasing even with H reached 5 T at 3 K (inset of Figure 3(b)). The lack of high-field saturation within *ab* plane suggests the presence of magnetic anisotropy in Dy (1). The observed magnetic anisotropy maybe root in the anisotropic coordination environment of Dy ions, as shown in Figure S11, and all the Cl^- ions that bounded with Dy ion are almost located within the honeycomb layer, which is perpendicular to the easy magnetization axis of the crystal.[20,21] Substitution of other rare-earth elements leads to similar observations but with different saturation magnetic fields and moments (Figure 3(c), Figure S13). The fitted effective magnetic moments and the theoretical values[22] are listed in Figure 3(d) and Table S5. The theoretical values of effective magnetic moments of trivalent rare-earth ions are described by $g_J\sqrt{\boldsymbol{J}(\boldsymbol{J}+1)}$, in that they have a $(2J+1)$-fold ground state, and the degeneracy being lifted by a magnetic field. Here g_J is Landé g_J factor, between 1 and 2 in value; the total angular momentum $\boldsymbol{J}$ is the sum of the orbital $\boldsymbol{L}$ and spin $\boldsymbol{S}$ momenta. The magnetic moments of trivalent rare-earth ions mainly depend on their J-values, which takes an asymmetric "m" shape as the atomic number increases. It is shown that except for Sm (1) and Eu (1), the μ_{eff} values of other compounds agree well with theoretical predictions. This indicates that the magnetic moments of most RE (1) compounds originate from the spin-orbit coupling of the $4f$ electrons for the rare-earth ions, while the Sm (1) and Eu (1) compounds may be in an excited state rather than the ground state due to the relatively small energy intervals ΔE between successive states. Therefore, the effect of the high excited states of the $\boldsymbol{L}$–$\boldsymbol{S}$ multiplet needs to be considered in the presence of a magnetic field rather than considering only the ground state for Sm (1) and Eu (1). Similar experimental results have also been reported.[23]

Lanthanide SMMs have been extensively studied for their single ion anisotropies and the ground state bistable with large m_J values due to strong spin-orbit coupling. Among the lanthanide ions, Dy^{3+}, Tb^{3+}, Er^{3+}, Ho^{3+} are more frequently used to construct SMMs, as their higher μ_{eff} is beneficial for realizing SMMs (Figure 3(c) and 3(d)). In paticular, Dy^{3+} is a Kramers ion (with odd-number of f-electrons), which reduces the requirement for ligand field symmetry to achieve high U_{eff} values (U_{eff} is the effective energy barrier relating to thermal activation to the relation of magnetization). As a result, Dy^{3+}-based SMMs have become the most studied category among lanthanide SMMs, and below we take Dy (1) as an example to study the SMM behavior in RE (1).

The SMMs behavior of Dy (1) is confirmed through measurements of AC magnetic susceptibility. The temperature dependences of the in-phase and out-of-phase AC susceptibilities (χ' and χ'') were measured under an oscillating field of 1.7 Oe within 100–10000 Hz. The slow relaxation of magnetization behavior is the most crucial characteristic for SMMs. In the high frequency region, the magnetic susceptibility of the SMM will lag behind the driving field, resulting in a phase shift, that is, χ'' starts to increase accompanied by a fall of χ'. Further increasing the frequency or decreasing the temperature, the magnetization begins to "block" and shows less response to the oscillating field, with a decrease of χ''. Figure 4(a) and 4(b) show both the maximum of χ'' and χ' shift towards higher temperature as the frequency increases under a bias magnetic field of 700 Oe, suggesting that Dy (1) is a field-induced SMM[3,24] (Figure S14 and S15). In the low frequency range of the measured AC magnetic susceptibility, two separate relaxation processes are clearly observed between 1.8 and 2.6 K (Figure 4(c) and Figure S16). The relaxation processes can be described by the sum of two modified Debye functions (1):[25]

$$\lambda_{ac}(w) = \frac{\lambda_2 - \lambda_1}{1 + (iw\tau_2)^{(1-\alpha_2)}} + \frac{\lambda_1 - \lambda_0}{1 + (iw\tau_1)^{(1-\alpha_1)}} + \lambda_0 \quad (1)$$

The parameters α in Equation (1) account for deviations from Debye process, and the results of the fitting are shown in Figure 4(c) and Table S6. The left semicircles in Figure 4-(c) are assigned to faster relaxation dynamic. We consider here direct, Orbach and Raman process for Dy (1), the temperature dependence of relaxation time can be fitted using the Equation (2), and the results is shown in Figure 4-(d).

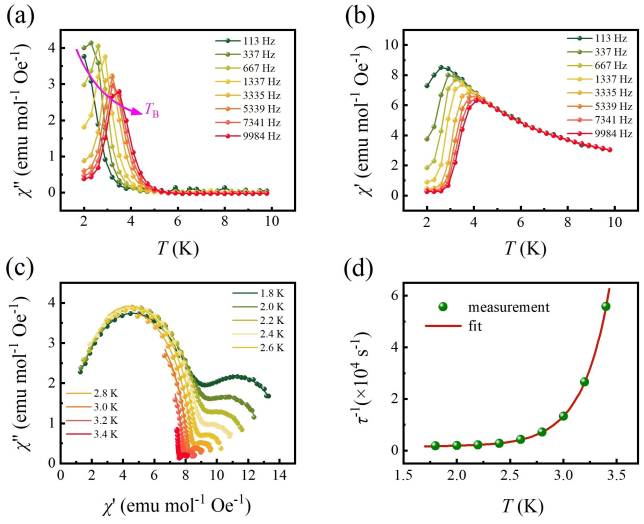

Figure 4. AC magnetic properties. Frequency dependence of the (a) out-of-phase and (b) in-phase magnetic susceptibility for Dy (1), collected under 700 Oe DC field at frequencies of $f = 100$ (green trace) to 10000 Hz (red trace) from 2 K to 10 K in 0.3 K intervals. (c) Cole-cole plots under 700 Oe DC field. The solid lines represent a best fit to a sum of two modified Debye functions (1). (d) Temperature dependence of the relaxation times extracted from the left semicircles in (c). The red solid line is the fitting result based on Equation (2).

$$\tau_1^{-1} = AT + \tau_0^{-1}\exp\left(-\frac{U_{eff}}{k_B T}\right) + CT^n \quad (2)$$

Where τ_0 is the relation time of Orbach process. The fitted curve is in good agreement with the experimental values of relaxation time of Dy (1) at different temperatures. The fitted $\tau_0 = 2.24 \times 10^{-9}$ s, lies in the typical range of 10^{-12} to 10^{-7} s for SMMs.[26] $U_{eff} = 141.65\ cm^{-1}$, indicates that Dy (1) has a lower effective energy barrier than many of other Dy-based SMMs,[2a] probably because the rare-earth groups do not have giant anisotropy.[20] The right semicircles suggest a slow relaxation process and is difficult to fit with above usual relaxation process. The nature of these slower and faster relaxation processes is most likely associated with two inequivalent Dy ions in the framework, as shown in some Dy^{III} based SMMs.[25b]

We have successfully synthesized a series of perovskites with rare-earth groups in the A sites, $(RECl_2(H_2O)_6)_2$-$(H_2dabco)_7$ $Cs_9Cl_{25}V_{Cl2}$ (RE (1), dabco = 1,4-diazabicyclo [2.2.2] octane, RE = rare-earths except Sc/Pm/Lu, V_{Cl} = anion vacancy), realizing the nanostructuring of SMMs in inorganic perovskite frameworks. Crystal structure determination and the electron density distributions analysis reveal the incorporated high density rare-earth groups are long-range ordered and chemically bonded to the inorganic perovskite framework. For Dy (1), the introduction of isolated rare-earth groups turns the compound into a SMM, with the easy magnetization direction perpendicular to the *ab* plane and large effective magnetic moment. Frequency and temperature dependence of χ' and χ'' demonstrate that Dy (1) is a field-induced SMM with two-step relaxation behavior. Substitution of other rare-earth elements leads to similar compounds and magnetic behaviors, with the effective magnetic moments generally agreeing well with the theoretical values of the corresponding trivalent rare-earth ions. This new method of accommodating SMMs into OMHP frameworks could be extended to generate a distinct family of multifunctional SMMs to improve material properties.

Acknowledgements

We thank Y. T. Song for his assistances in the single crystal X-ray diffraction measurements, X. F. Wang and Q. Fang for their assistances in sample preparation. This work is financially supported by the National Key Research and Development Program of China (Grant No. 2018YFE0202600), the National Natural Science Foundation of China (Grant No. 52272268), the Key Research Program of Frontier Sciences, CAS (Grant No. QYZDJ-SSW-SLH013), the Informatization Plan of Chinese Academy of Sciences (Grant No. CAS-WX2021SF-0102) and the Youth Innovation Promotion Association of CAS (Grant No. 2019005).

Conflict of Interest

The authors declare no conflict of interest.

Data Availability Statement

The data that support the findings of this study are available from the corresponding author upon reasonable request.

Keywords: Framework · Magnetic Materials · Nanostructuring · Organic Metal Halide Perovskites

[1] A. Gaita-Ariño, F. Luis, S. Hill, E. Coronado, *Nat. Chem.* **2019**, *11*, 301–309.
[2] a) D. N. Woodruff, R. E. Winpenny, R. A. Layfield, *Chem. Rev.* **2013**, *113*, 5110–5148; b) C. Papatriantafyllopoulou, E. E. Moushi, G. Christou, A. J. Tasiopoulos, *Chem. Soc. Rev.* **2016**, *45*, 1597–1628.
[3] J. M. Frost, K. L. M. Harriman, M. Murugesu, *Chem. Sci.* **2016**, *7*, 2470–2491.
[4] A. Caneschi, D. Gatteschi, R. Sessoli, A. L. Barra, L. C. Brunel, M. Guillot, *J. Am. Chem. Soc.* **1991**, *113*, 5873–5874.
[5] R. Sessoli, D. Gatteschi, A. Caneschi, M. A. Novak, *Nature* **1993**, *365*, 141–143.
[6] a) H. Li, P. Jing, J. Lu, L. Xi, Q. Wang, L. Ding, W. M. Wang, Z. Song, *Dalton Trans.* **2021**, *50*, 2854–2863; b) D. Errulat, R. Marin, D. A. Galico, K. L. M. Harriman, A. Pialat, B. Gabidullin, F. Iikawa, O. D. D. Couto Jr., J. O. Moilanen, E. Hemmer, F. A. Sigoli, M. Murugesu, *ACS Cent. Sci.* **2019**, *5*, 1187–1198; c) T. Sato, B. K. Breedlove, M. Yamashita, K. Katoh, *Angew. Chem. Int. Ed.* **2021**, *60*, 21179–21183; *Angew. Chem.* **2021**, *133*, 21349–21353; d) R. Marin, G. Brunet, M. Murugesu, *Angew. Chem. Int. Ed.* **2021**, *60*, 1728–1746; *Angew. Chem.* **2021**, *133*, 1752–1772.

[7] L. Bogani, W. Wernsdorfer, *Nat. Mater.* **2008**, *7*, 179–186.
[8] a) J. L. Liu, Y. C. Chen, M. L. Tong, *Chem. Soc. Rev.* **2018**, *47*, 2431–2453; b) F. S. Guo, B. M. Day, Y. C. Chen, M. L. Tong, *Science* **2018**, *362*, 1400–1403.
[9] a) A. Cornia, M. Mannini, P. Sainctavit, R. Sessoli, *Chem. Soc. Rev.* **2011**, *40*, 3076–3091; b) N. Domingo, E. Bellido, D. Ruiz-Molina, *Chem. Soc. Rev.* **2012**, *41*, 258–302.
[10] R. V. Martínez, F. García, R. García, E. Coronado, A. Forment-Aliaga, F. M. Romero, S. Tatay, *Adv. Mater.* **2007**, *19*, 291–295.
[11] C. Gimenez-Lopez Mdel, F. Moro, A. La Torre, C. J. Gomez-Garcia, P. D. Brown, J. van Slageren, A. N. Khlobystov, *Nat. Commun.* **2011**, *2*, 407.
[12] a) D. Aulakh, J. B. Pyser, X. Zhang, A. A. Yakovenko, K. R. Dunbar, M. Wriedt, *J. Am. Chem. Soc.* **2015**, *137*, 9254–9257; b) D. Aulakh, H. Xie, Z. Shen, A. Harley, X. Zhang, A. A. Yakovenko, K. R. Dunbar, M. Wriedt, *Inorg. Chem.* **2017**, *56*, 6965–6972; c) D. Aulakh, L. Liu, J. R. Varghese, H. Xie, T. Islamoglu, K. Duell, C. W. Kung, C. E. Hsiung, Y. Zhang, R. J. Drout, O. K. Farha, K. R. Dunbar, Y. Han, M. Wriedt, *J. Am. Chem. Soc.* **2019**, *141*, 2997–3005; d) T. Liu, Z. Fan, Z. Mi, W. Du, X. Song, R. Liu, H. Wang, Y. Du, *J. Solid State Chem.* **2022**, *305*, 122697.
[13] a) M. V. Kovalenko, L. Protesescu, M. I. Bodnarchuk, *Science* **2017**, *358*, 745–750; b) S. Macpherson, T. A. S. Doherty, A. J. Winchester, S. Kosar, D. N. Johnstone, Y. H. Chiang, K. Galkowski, M. Anaya, K. Frohna, A. N. Iqbal, S. Nagane, B. Roose, Z. Andaji-Garmaroudi, K. W. P. Orr, J. E. Parker, P. A. Midgley, K. M. Dani, S. D. Stranks, *Nature* **2022**, *607*, 294–300; c) D. Yang, B. Zhao, T. Yang, R. Lai, D. Lan, R. H. Friend, D. Di, *Adv. Funct. Mater.* **2022**, *32*, 2109495; d) P. Odenthal, W. Talmadge, N. Gundlach, R. Wang, C. Zhang, D. Sun, Z.-G. Yu, Z. Valy Vardeny, Y. S. Li, *Nat. Phys.* **2017**, *13*, 894–899; e) Y. Zhang, E. Parsonnet, A. Fernandez, S. M. Griffin, H. Huyan, C.-K. Lin, T. Lei, J. Jin, E. S. Barnard, A. Raja, P. Behera, X. Pan, R. Ramesh, P. Yang, *Sci. Adv.* **2022**, *8*, eabj5881; f) B. Saparov, D. B. Mitzi, *Chem. Rev.* **2016**, *116*, 4558–4596; g) W.-Q. Liao, D. Zhao, Y.-Y. Tang, Y. Zhang, P.-F. Li, P.-P. Shi, X.-G. Chen, Y.-M. You, R.-G. Xiong, *Science* **2019**, *363*, 1206–1210.
[14] a) Z. Zhao, F. Gu, H. Rao, S. Ye, Z. Liu, Z. Bian, C. Huang, *Adv. Energy Mater.* **2019**, *9*, 1802671; b) Y. Han, S. Yue, B. B. Cui, *Adv. Sci.* **2021**, *8*, 2004805.
[15] L. A. Paton, W. T. Harrison, *Angew. Chem. Int. Ed.* **2010**, *49*, 7684–7687; *Angew. Chem.* **2010**, *122*, 7850–7853.
[16] Deposition number 2239241 contains the supplementary crystallographic data for this paper. These data are provided free of charge by the joint Cambridge Crystallographic Data Centre and Fachinformationszentrum Karlsruhe Access Structures service.
[17] K. Momma, F. Izumi, *J. Appl. Crystallogr.* **2011**, *44*, 1272–1276.
[18] K. Momma, T. Ikeda, A. A. Belik, F. Izumi, *Powder Diffr.* **2013**, *28*, 184–193.
[19] J. D. Rinehart, M. Fang, W. J. Evans, J. R. Long, *Nat. Chem.* **2011**, *3*, 538–542.
[20] J. P. Sutter, V. Bereau, V. Jubault, K. Bretosh, C. Pichon, C. Duhayon, *Chem. Soc. Rev.* **2022**, *51*, 3280–3313.
[21] S.-D. Jiang, S.-X. Qin, *Inorg. Chem. Front.* **2015**, *2*, 613–619.
[22] a) R. Kubo, *Solid State Physics*, McGraw-Hill, New York, **1969**; b) C. Kittel, *Introduction To Solid State Physics-Eight Edition*, Suzanne Ingrao, United States of America, **2004**.
[23] a) J. Hölsä, M. Lastusaari, J. Niittykoski, R. Sàez Puche, *Phys. Chem. Chem. Phys.* **2002**, *4*, 3091–3097; b) T. Taniguchi, W. Iizuka, Y. Nagata, T. Uchida, H. Samata, *J. Alloys Compd.* **2003**, *350*, 24–29; c) D. Ranaut, K. Mukherjee, *arXiv* **2022**, https://doi.org/10.48550/arXiv.2210.02007.
[24] a) P. E. Car, M. Perfetti, M. Mannini, A. Favre, A. Caneschi, R. Sessoli, *Chem. Commun. (Camb.)* **2011**, *47*, 3751–3753; b) J. J. Le Roy, M. Jeletic, S. I. Gorelsky, I. Korobkov, L. Ungur, L. F. Chibotaru, M. Murugesu, *J. Am. Chem. Soc.* **2013**, *135*, 3502–3510; c) P. H. Lin, I. Korobkov, T. J. Burchell, M. Murugesu, *Dalton Trans.* **2012**, *41*, 13649–13655.
[25] a) M. Grahl, J. Kötzler, I. Seßler, *J. Magn. Magn. Mater.* **1990**, *90–91*, 187–188; b) Y.-N. Guo, G.-F. Xu, P. Gamez, L. Zhao, S.-Y. Lin, R. Deng, J. Tang, H.-J. Zhang, *J. Am. Chem. Soc.* **2010**, *132*, 8538–8539.
[26] X. N. Yao, J. Z. Du, Y. Q. Zhang, X. B. Leng, M. W. Yang, S. D. Jiang, Z. X. Wang, Z. W. Ouyang, L. Deng, B. W. Wang, S. Gao, *J. Am. Chem. Soc.* **2017**, *139*, 373–380.

Manuscript received: January 10, 2023
Accepted manuscript online: February 13, 2023
Version of record online: March 3, 2023